In Silico Assessment of Drug Safety in Human Heart Applied to Late Sodium Current Blockers

Beatriz Trenor[1], Julio Gomis-Tena[1], Karen Cardona[1], Lucia Romero[1], Sridharan Rajamani[2], Luiz Belardinelli[2], Wayne Giles[3], Javier Saiz[1]

[1]Instituto de Investigación Interuniversitario en Bioingeniería y Tecnología Orientada al Ser Humano (I3BH), Universitat Politècnica de València (UPV), Spain

[2]Department of Biology (Cardiovascular Therapeutic Area), Gilead Sciences, Fremont, CA

[3]University of Calgary, Canada

Short title: Simulation Tool to Assess Drug Safety

Contact information:

Beatriz Trenor, PhD.

Departamento de Ingeniería Electrónica

Universitat Politècnica de València

Camino de Vera s/n

46022 Valencia, SPAIN

Ph: +34 96 3877007 ext. 76086; Fax: +34 96 3877093

Email:btrenor@eln.upv.es

CONFLICTS OF INTEREST

Funding for some of the work was provided by Gilead Science Ltd in the form of an unrestricted grant to investigators at Universitat Politècnica de València.

KEYWORDS: anti-arrhythmic, drug safety, multi-channel block, reverse rate-dependence, late sodium current, transmural dispersion of repolarization.

Abbreviations:

AP, action potential

APD, action potential duration

EAD, early afterdepolarization

IC_{50}, half inhibition concentration

I_{Kr}, rapidly activating rectifying K^+ current (hERG)

I_{Ks}, slowly activating rectifying K^+ current

I_{NaL}, late sodium current

I_{K1}, inward rectifying K^+ current

I_{net}, net membrane current

LQT3, long QT 3

pIC_{50}, $-\log_{10}IC_{50}$

QT_{int}, QT interval

RRD, reverse rate-dependence

SF, safety factor for conduction

TDR, transmural dispersion of repolarization

GS967, (6-(4-(trifluoromethoxy) phenyl)-3-(trifluoromethyl)-[1,2,4]triazolo[4,3-a]pyridine)

ABSTRACT

Drug-induced action potential (AP) prolongation leading to Torsade de Pointes is a major concern for the development of anti-arrhythmic drugs. Nevertheless the development of improved anti-arrhythmic agents, some of which may block different channels, remains an important opportunity. Partial block of the late sodium current (I_{NaL}) has emerged as a novel anti-arrhythmic mechanism. It can be effective in the settings of free radical challenge or hypoxia. In addition, this approach can attenuate pro-arrhythmic effects of blocking the rapid delayed rectifying K^+ current (I_{Kr}). The main goal of our computational work was to develop an in-silico tool for preclinical anti-arrhythmic drug safety assessment, by illustrating the impact of I_{Kr}/I_{NaL} ratio of steady-state block of drug candidates on "torsadogenic" biomarkers. The O'Hara et al. AP model for human ventricular myocytes was used. Biomarkers for arrhythmic risk, i.e. AP duration, triangulation, reverse rate-dependence, transmural dispersion of repolarization, and electrocardiogram QT intervals were calculated using single myocyte and one-dimensional strand simulations. Predetermined amounts of block of I_{NaL} and I_{Kr} were evaluated. "Safety plots" were developed to illustrate the value of the specific biomarker for selected combinations of IC_{50}s for I_{Kr} and I_{NaL} of potential drugs. The reference biomarkers at baseline changed depending on the "drug" specificity for these two ion channel targets. Ranolazine and GS967 (a novel potent inhibitor of I_{NaL}), yielded a biomarker data set that is considered safe by standard regulatory criteria. This novel in-silico approach, is useful for evaluating pro-arrhythmic potential of drugs and drug candidates in the human ventricle.

INTRODUCTION

The emerging importance of the role of an enhanced late sodium current (I_{NaL}) in mammalian ventricle as a contributor to the pathogenesis of acquired and hereditary disease has resulted in this current being a target for anti-arrhythmic drug development. Under relatively common pathological conditions, I_{NaL} density is enhanced significantly (2 to 5-fold) in ventricle. These conditions include: heart failure, oxidative stress, hypoxia, ventricular hypertrophy and LQT-related mutations. When I_{NaL} is increased, the action potential duration (APD) of human ventricular myocytes lengthens.[1-3] This may lead to initiation and/or maintenance of arrhythmias such as Torsade de Pointes (TdP).[4,5] In all such cases the repolarization reserve is reduced.

Several experimental and clinical studies have demonstrated significant anti-arrhythmic effects of I_{NaL} blockers, such as ranolazine.[6-9] However, ranolazine and other compounds in development, which are relatively selective for I_{NaL}, may also block other ion channels such as delayed rectifier potassium channels (I_{Kr}). This effect can result in action potential (AP) prolongation.[7] Recently, a potent and selective inhibitor of cardiac I_{NaL}, GS967, has been reported to suppress experimental arrhythmias in female rabbits.[10] It is a requirement of the process of drug development to evaluate the ratio for I_{NaL}/I_{Kr} blockade for this drug candidate.

For this purpose, detailed understanding of the role of the ionic currents involved in the different phases of AP repolarization (early, intermediate and late phases) is essential. The delicate balance of the small ionic currents which underlie the AP plateau determines the impact of these drugs on APD prolongation, and other biomarkers for arrhythmic risk (e.g. AP triangulation). Although several experimental and theoretical studies of this have yielded substantial information,[11-21] further investigation based on

data and principles from human ventricle is required to fully understand ionic mechanisms underlying drug-induced changes in APD.

It is noteworthy that APD prolongation alone appears to be insufficient to define "torsadogenic" risk.[22] Additional biomarkers for arrhythmic risk must be identified and evaluated when defining anti-arrhythmic drug safety. Indeed, changes in QT interval (QT_{int}), reverse rate-dependence (RRD) of APD prolongation, and transmural dispersion of repolarization (TDR) have been also proposed as "torsadogenic" indicators.[22-24]

Within the past three years, computer simulations have been employed in drug development programs with the goal of assessing in silico risk for drug-induced cardiac arrhythmia.[25-28] However, only Mirams et al.[25] and Sarkar et al.[29] utilized human AP models, in addition to models of the rabbit and dog ventricular APs.

The main goals of this project were to identify the relative role of ionic currents at defined phases of repolarization in human ventricle, and to use this information to reveal and to illustrate the impact of I_{NaL} and I_{Kr} block on selected biomarkers which define arrhythmic risk. Our analysis reveals the biophysical basis for reverse rate-dependence in human ventricle. In addition, a new simulation tool denoted the "safety plot" is developed and utilized to assess drug safety for I_{NaL} blockers.

RESULTS

Effects of I_{NaL} and I_{Kr} Block on Repolarization of Diseased Human Ventricular AP

Single isolated myocyte simulations were conducted to reveal the effetcs of ranolazine and GS967 on AP waveform, and to study the changes of several "plateau" ionic currents at defined stages during repolarization. Figure 1(A) shows the APs for baseline (left), together with the effects of ranolazine (centre) and GS967 (right). Control AP is also shown (see dashed lines) in the three cases for reference. Ranolazine had no significant effects, apparently, changing APD_{30} to 100.9%, APD_{60} to 103% and APD_{90} to 105% of baseline values. In contrast, GS967 decreased APD_{30} to 86.9%, APD_{60} to 87.2%, and APD_{90} to 91.1% of baseline. The higher selectivity of GS967 for I_{NaL} (IC_{50} of 0.13 μM and >10 μM for I_{NaL} and I_{Kr}, respectively)[10] compared with ranolazine, can account for its effect on APD compared to ranolazine. The differences in the changes of APD at the selected phases of repolarization can be explained by the different sizes and functional roles of the repolarization currents. For example, Figure 1(B) shows the small role of I_{NaL} at 90% of repolarization, but also illustrates the more important role of the current at 30% and 60%. A similar pattern also holds for I_{Kr} and I_{Ks} (panel C) at 90% of repolarization. However, the waveform of repolarization also depends on the delicate balance of many other ionic currents (e.g. I_{K1}, I_{CaL}). Thus, the I_{net} (Figure 1E) is a key variable to "track". In general, in human ventricle a relatively specific drug for I_{NaL} has greater effects on the early phase of repolarization. This effect on early as opposed to late repolarization has been termed an increase in triangulation.[24]

Rate-dependent Effects of I_{NaL} and I_{Kr} Block on Repolarization

To begin to explore the effects of I_{NaL} and I_{Kr} blockers on rate-dependent APD changes, APs at two different steady-state stimulation frequencies were simulated. Test compounds with different degrees of specificity for the selected ion channels were

"applied" by varying the IC_{50} for I_{NaL} and I_{Kr}. In all the cases the amount of block was calculated for a drug at a concentration of 5 μM. Figure 2 shows APs and several underlying ionic currents for a basic cycle length (BCL) 500 ms (continuous trace) and 2000 ms (discontinuous trace). The superimposed data depict (i) baseline (column 1), (ii) in the presence of a drug specific for I_{Kr} (IC_{50} of 10^{-5} and 10^{-3} M for I_{Kr} and I_{NaL}, respectively) in column 2, (iii) a drug specific for I_{NaL} (IC_{50} of 10^{-3} and 10^{-7} M for I_{Kr} and I_{NaL}, respectively) in column 3, and (iv) a drug with the same specificity for these two ion channels (IC_{50} of 10^{-5} M for I_{Kr} and I_{NaL}) in column 4. As expected, these results demonstrate that a drug more specific for I_{Kr} (column 2) prolongs APD_{90} and this effect is larger at low frequencies (discontinuous trace) than at high frequencies (continuous trace), 124% and 118% of baseline at 0.5 Hz and 2 Hz, respectively. The so-called reverse rate-dependence effect exerted by I_{Kr} blockers, i.e. a greater APD prolongation at low frequencies (see Figure 2 panel C), can be in part explained by I_{Ks} accumulation at the higher frequency (residual activation), as experimentally observed by others.[30] We note how in the O'Hara et al.[31] (ORd) model the contribution of I_{Kr} does not change significantly with frequency. I_{Ks} is larger at the higher frequency due to residual activation.

Note that if the drug is more selective for I_{NaL} (column 3), APD_{90} is further shortened at low frequencies (69% and 78% of baseline value at 0.5 Hz and 2 Hz, respectively). This is because the contribution of I_{NaL} to net current is relatively large at low frequencies.

When the drug has the same specificity for I_{NaL} and I_{Kr} (column 4), the changes in APD_{90} are similar for both cycle lengths (113% and 112% of baseline value at 0.5 Hz and 2 Hz, respectively). Note that the reverse rate-dependence effect due to I_{Kr} block is neutralized by I_{NaL} block, as has been observed in rabbit ventricular myocytes.[32] This

pattern of changes holds for APD_{30} and APD_{60}. Our results show that the I_{NaL}/I_{Kr} ratio of blockade of potential drugs has an important effect on reverse rate-dependence, which is an indicator to evaluate drug safety.

To further investigate the ionic mechanisms of reverse rate-dependence observed in the presence of I_{NaL} and I_{Kr} blockers, we calculated the net current. Indeed, as postulated by Banyasz et al.[33], RRD is an intrinsic property of these human ventricular cells; stimulus frequency modulates APD, so that at low frequencies APD is longer. In all cases, when APD is long, the net current is very small. As a consequence, any change in the very small net current (e.g. due to drug effect) causes prominent changes in APD. The opposite effects take place at high frequencies when APD is shorter and the net outward current is larger. We computed the net current at the instant of time corresponding to APD_{60} for the four cases considered in Figure 2 (baseline, drug 1, 2, and 3), always assuming 5 μM of the drugs with variable specificities for I_{NaL} and I_{Kr}. These changes were evaluated at different steady-state cycle lengths (from BCL 500 ms to 2000 ms). The relationship between the net current and the APD_{90} is illustrated in Figure 3. These results are in accordance with experimental observations of Banyasz et al.[33]: that is, longer APDs tend to correspond to lower net currents regardless of the drug used.

APD and Rate Dependence Safety Plots

As described above, our results show the I_{NaL}/I_{Kr} ratio of blockade of potential drugs has an important effect on rate-dependent changes in APD. To illustrate this, multiple sets of ventricular myocyte simulations were carried out at different but constant stimulation frequencies for selected combinations of I_{NaL} and I_{Kr} blockade. Potential drugs having IC_{50} for I_{Kr} in the range 10^{-6} to 10^{-3} M, and IC_{50} for I_{NaL} in the range 10^{-7} to 10^{-3} M were tested at a fixed 5 μM concentration. The effects of different

concentrations (3, 5, and 8 μM) at a stimulation frequency of 1 Hz can be observed in supplemental Figure S2.

Figure 4 illustrates these findings in the form of a safety plot, using a color scale for APD_{90} values. Relatively large values for the biomarker (APD_{90}) are represented in red, and relatively small APD values are shown in blue. The circle represented in bottom right corner corresponds to the baseline condition (I_{NaL} is enhanced two-fold). Here, essentially no current block takes place (a pIC_{50} results in 0.995 of I_{NaL} and I_{Kr}). APD_{90} is 353.3 ms in this case. Consideration of data in the right edge of the safety plot, shows that when I_{NaL} is progressively blocked (IC_{50} for I_{NaL} decreases, and thus pIC_{50} increases) the biomarker decreases (APD_{90} is 252.1 ms in the top right corner). Data to the left in the bottom edge, corresponding to a progressive block of I_{Kr} (IC_{50} for I_{Kr} decreases, and pIC_{50} increases), lead to an increase of the the biomarker (APD_{90} is 741.2 ms with the induction of an early-after depolarization (EAD) in the left bottom corner).

But what happens for other combinations of block? Where is the safety barrier? Black lines join the IC_{50} combinations for which the biomarker is 120%, 110%, 100%, and 90% of baseline value, represented in the bottom right corner. The 90% barrier, would depict beneficial effects of the drug, as the biomarker is reduced. In contrast, biomarker values which fall to the left side of the 110% barrier implies dangerous effects of the drug increasing the biomarker.

Figure 5 represents safety plots using APD_{90}, APD_{60}, APD_{30}, and triangulation as biomarkers, and the safety plots in Figure 6 illustrate the rate-dependence, i.e. the effect of a BCL change on APD_{90}. Ranolazine, represented by the black circle, can be positioned in the matrix, based on its approximately IC_{50} of 6 and 12 μM for I_{NaL} and I_{Kr}, respectively. Note that this drug is located in the "safe" part of the matrix. Also the

test compound GS967 (IC_{50} of 0.13 and >10 μM for I_{NaL} and I_{Kr}, respectively), represented by a black triangle, is apparently safer than ranolazine. At high frequencies (first column) shorter APDs and triangulation (blue and green colors) are observed. In contrast, the results at low frequencies (2nd column) show longer APDs (red and yellow colors). As expected, the decrease in APD exerted by GS967 is more pronounced at low frequencies and especially APD_{30}, whereas the slight increase of APD exerted by ranolazine does not result in any significant changes (approximately 110% of the baseline value).

AP triangulation data (panel D of Figure 5) reveal that both ranolazine and GS967 slightly increase this parameter with respect to the baseline value. Specifically, ranolazine further increases APD_{90} more than APD_{30}, whereas GS967 decreases APD_{30} more than APD_{90}, at each stimulus rate.

Finally, Figure 6 highlights that drugs very specific for I_{NaL} (such as GS967) decrease APD_{90}, APD_{60}, and APD_{30} rate-dependence, calculated as the difference between APD at minimum frequency and APD at maximum frequency. In the case of ranolazine, the rate dependence (RD) is unchanged (100% of baseline), due to the fact that the block of I_{Kr} would provoke large reverse rate-dependence, which is neutralized by the concomitant block of I_{NaL} by the drug.

Effects of I_{NaL} and I_{Kr} blockers on QT interval and Transmural Dispersion of Repolarization

Simulations were carried out at tissue level based on an in silico fiber of 165 cells composed of a fixed number of endocardial, M, and epicardial cells as described in O'Hara et al.[31] Pseudo-ECGs were computed and the corresponding QT intervals were measured. In addition, repolarization times of selected myocytes within the fiber were calculated, and transmural dispersion of repolarization was defined as the difference

between the maximum and the minimum repolarization times in the fiber. Figure 7 panel A shows APs measured in the central cells of each part of the tissue (endo-, midmyo-, and epicardial tissues) under baseline conditions (left), in the presence of 5 μM ranolazine (centre) or GS967 (right). Panel B shows the pseudo-ECG for these conditions. Note that QT interval was increased slightly by ranolazine (107% of the baseline value) but was decreased by GS967 (91.4% of the baseline value). Finally, repolarization times at selected myocytes within the fiber are depicted in Figure 7 panel C and TDR is indicated in the curves. Note that ranolazine and GS967 decreased TDR to 81.5% and 54.2% of the baseline value, respectively.

Safety Plots Based on QT Interval and Transmural Dispersion of Repolarization data

Figure 8 summarizes the values of QT_{int} and TDR for different combinations of I_{Kr} and I_{NaL} blockade in different safety plots for 3 μM (left), 5 μM (centre), and 8 μM (right) of potential drugs. The reference QT_{int} and TDR correspond to the baseline conditions (right bottom corner). The results obtained in our simulations indicate that GS967 is safer than ranolazine, as it reduces the QT_{int} down to 90% of its baseline value for the lower concentration.

With regard to the TDR simulations shown in Figure 8 panel B, the two drugs that were assessed reduced TDR quite significantly. This is of interest as TDR is being seriously considered an important biomarker for arrhythmic risk, and very few studies have tested the effects of drugs on this biomarker. The reduction of the TDR exerted by these drugs is notable, highlighting their beneficial effects.

DISCUSSION

Major Findings

Our computational work, based on a current and very comprehensive mathematical model of the human ventricular AP, provides novel insights into the roles of I_{NaL} and I_{Kr} block in the modulation of well accepted biomarkers for pro-arrhythmic risk. Our approach further illustrates and documents the utility of computational methods as one potential assessment tool in Safety Pharmacology. The principal findings and insights from our work are: (i) demonstration that it is essential to study the role of selected drug targeted currents (I_{NaL}, I_{Kr}, I_{Ks}) at defined time points of AP repolarization, (ii) novel insight into the ionic mechanisms responsible for reverse rate-dependence of anti-arrhythmic agents: delayed rectifier K^+ currents exhibit a relatively large effect on the net current which governs the initiation of repolarization and modulates the repolarization waveform, (iii) demonstration of importance of drug-induced APD prolongation assessed at steady-state, (iv) an explanation of how selective partial block of I_{NaL} confers significant anti-arrhythmic effects in terms of reduction of APD, RRD of APD prolongation, QT interval or TDR, (v) integration of experimental data sets in terms of safety plots to illustrate that the ratios of block of I_{NaL}/I_{Kr} (measured as IC_{50} values) for a drug is a novel mechanism-based tool, that can be used to advantage during the initial phases of drug development.

Mechanisms for Reverse-Rate Dependence of Drug-induced APD Prolongation

The repolarization of AP is determined by the very delicate balance of ionic currents.[34] A very small change in this balance (net current) caused by a drug may have important consequences on AP morphology and thus on myocyte electrophysiological properties. This concept was first recognized by classical cardiac electrophysiologists[34] and originally was termed all-or-none repolarization. Many subsequent studies have

provided basis for understanding the ionic mechanisms for repolarization, and the concept of repolarization reserve, through mathematical modeling.[13,35] The main goal of the present study (oriented to I_{NaL} and I_{Kr} block) was to reveal the effects of established or in development anti-arrhythmic drugs on repolarization in human ventricle using computational methods. Our results show that a new and very selective blocker for I_{NaL} (GS967) has a relatively large effect on the early phase of repolarization (significant decrease of APD_{30}) in comparison with its effects on the late phase of repolarization (APD_{90}) whereas other currents, e.g. I_{K1}, strongly modulate APD_{90}. Similar pattern of results has been reported,[10] where GS967 reduced APD_{50} more than APD_{90} in isolated rabbit myocytes. Previously, somewhat similar results were obtained by Goineau et al.[36] in rabbit Purkinje fibers. Lidocaine increased AP triangulation, by reducing APD_{30} more than APD_{90}. These findings show that the net impact on AP morphology must be evaluated as a net balance of multiple ion channel conductances. In our simulations, as demonstrated in the safety plots of Figure 5, the changes in triangulation due to I_{NaL} block also depend on the amount of I_{Kr} block, i.e. on the drug specificity. If we consider a pure I_{NaL} blocker (moving upwards in the right edge of the safety plots of Figure 5 panel D) AP triangulation tends to diminish as specificity for I_{NaL} increases. Figure 2 illustrates a plausible ionic mechanism for this. The observed decrease in AP triangulation in response to selective blockers of I_{NaL} is in accordance with the experimental observation that agents that enhance I_{NaL} have the opposite effect: an increase in triangulation.[37,38] Our results also provide insight into a previous paper that reported an increase in AP triangulation following selective I_{Kr} block.[39]

Another new mechanistic insight from our simulations is that the ratio I_{NaL}/I_{Kr} of block by drug candidates can strongly influence the drug-induced RRD of the APD even under steady-state conditions. Most contemporary drug discovery or Safety

Pharmacology initiatives consider RRD as an important biomarker for pro-arrhythmic actions.[22,23,40] It is well known that class III antiarrhythmic agents, such as dofetilide and other selective blockers of I_{Kr} include RRD effects.[30,41] RRD in human ventricle was reproduced by our simulations (see Figure 6). Specifically, our results showed that selective block of I_{NaL} led to APD shortening in a RRD manner, in accordance with experimental studies.[32] These counteracting actions lead to a neutralization of the reverse rate-dependence of APD prolongation when a drug blocks both I_{NaL} and I_{Kr}.[5,32] Similar effects have been reported in the setting of simultaneous block of I_{Kr} and I_{CaL}.[42] In summary, the delicate and dynamic balance between I_{Kr} and I_{NaL} block as a consequence of any relative affinity (IC_{50}) differences for ion channel targets can explain RRD of APD in human ventricle.

Several hypotheses have been developed to explain the underlying ionic mechanisms for reverse RRD modulation of APD. It was first postulated that I_{Ks} accumulation (that is, residual activation) observed at relative high frequencies in guinea-pig myocytes was responsible due to the slow deactivation kinetics of this current.[30,43] A somewhat similar phenomenon and species-dependent (see O'Hara et al.[44]) can be observed in our results (Figure 2), showing a steeper I_{Ks} increase at fast rates. Here, the kinetics of I_{Ks} could be a significant factor for the RRD of APD prolongation exerted by I_{Kr} blockers. However, I_{Ks} cannot be the only cause of RRD. Thus, even in the setting of I_{Ks} block by HMR1556, RRD APD prolongation was also observed in canine ventricular myocytes.[45]

Quite recently, Banyasz et al. have suggested that RRD was an intrinsic property of human ventricular cells.[33] Indeed, at low frequencies, when APD is relatively long, the net repolarizing current is very small. Under these conditions any change in the plateau currents can lead to significant changes in APD. Our results provide insight into

this. Note that the calculated curvi-linear relationship of the net current correlates strongly with APD_{90} (Figure 3). We conclude that in human ventricle intrinsic biophysical properties of I_{Kr} and I_{Ks} and their combined contribution to I_{net} result in the basis for reverse rate-dependence of APD.

Safety of I_{NaL} Blockers

Drug-induced APD prolongation, the associated dispersion in transmural repolarization in the human ventricle, and TdP inducibility have emerged as significant concerns in drug safety evaluations. Incresases in these parameters can be a major obstacle for drug approval.[46] In this context, I_{NaL} is emerging as a promising pharmacological target. Inhibition of this component of Na^+ current markedly reduces the TdP inducing capability of agents that prolong the QT interval.[5] Furthermore, I_{NaL} block is likely to have an additional anti-arrhythmic effect, especially in conditions which are characterized by enhanced I_{NaL} due to genetic or acquired causes. These include: LQT3, heart failure, hypoxia, and free radical challenge.[6,47,48-51]

Our simulations demonstrate that selective block of I_{NaL} (GS967) can decrease well-accepted biomarkers for arrhythmic risk. These include: APD, reverse rate-dependence, triangulation, QT_{int}, and transmural dispersion of repolarization. This insight is in accordance with experimental findings.[10,52] Indeed, Belardinelli et al.[10] have reported that in rabbit ventricular myocytes, GS967 almost completely restored the normal APD after it had been markedly increased with ATXII. In control conditions, GS967 had a slight tendency to decrease APD, with the effect being larger for APD_{50} than for APD_{90}.[10] There is also ample experimental and theoretical evidence that I_{NaL} enhancement can have opposite pro-arrhtyhmic effects, including an increase of triangulation,[53] reverse rate-dependence of APD prolongation measured in transgenic mice with LQT3[47] or the peak to end interval of the T-wave, which closely

approximates TDR, in rabbit ventricular wedges.[5] Perhaps more importantly, many experimental studies have shown that inhibition of I_{NaL} can markedly reduce the risk of drug-induced TdP, e.g. by I_{Kr} blockers. Thus, the combined application of I_{NaL} blockers with I_{Kr} blockers can improve the safety profile.[5,32,42,54-56] This concept was firstly illustrated by the simulation work of Noble et al.[57] and is confirmed by our computational results. Note that ranolazine suppressed early afterdepolarizations (EADs) and reduced the increase in TDR induced by the selective I_{Kr} blocker *d*-sotalol in canice cardiac wedges.[56] However, the net effect and clinical consequence of multiple channel blockade (mainly I_{Kr} and I_{NaL}) by ranolazine is a modest increase in the mean QT interval by 2–6 ms.[56,58] This important experimental observation was also reproduced by our results (see Figure 8), whereas more selective blockers of I_{NaL} (such as GS967) reduced QT interval.

Safety Plots as a Tool for Anti-arrhythmic Drug Development

At present, the preclinical assessment of drug-induced ventricular arrhythmia, a major concern for the international cardiac safety pharmacology community, is based mainly on experimental studies. Recently, however, advanced computational technology for in-silico assessment of the efficacy and safety of specific drugs has emerged as a complementary and potentially valuable tool.[28,29,59]

Notable research efforts have been made to link molecular dynamics to biophysical models.[60] Other detailed models of drug/ion-channel interaction take into account the rate of binding and unbinding[61] and can be reproduced in either Hodgkin-Huxley or Markov models formulations.[28,62,63] For example a recent study on the atrial-selectivity of ranolazine is based on a markovian model of its inhibiting effects on the sodium channels.[64,65]

In the present study we have used a classical measure of the drug action, by employing IC_{50} data, that is the fraction of block of the targeted channel conductance. A recent computational study by Mirams et al.[25] provided interesting insights into TdP prediction following simultaneous applications of many different ion channel blockers. Other computational studies have assessed the effects of I_{Ks} and/or I_{Kr} blockers on several biomarkers for arrhythmic risk as a proof of concept in the preclinical phase of development of drugs.[26,27,66] Our work complements and extends these approaches. We have evaluated for the first time the safety of drugs with different ratios of I_{NaL}/I_{Kr} block, using a recent and very detailed human AP model. Safety was estimated by accepted torsadogenic indicators: APD prolongation, triangulation, reverse rate-dependence, QT_{int}, and TDR.[22-24] The sizes and shapes of the safety zones vary from one biomarker to the other, but a general pattern of behavior can be observed: as the affinity for I_{NaL} block increases, safety (blue and green colors) increases. We note that the safety plot corresponding to the biomarker AP triangulation has the most extense unsafe zone, whereas TDR safety plots have the smallest unsafe zones. In our simulated safety plots a two-fold enhancement of I_{NaL} was considered. Based on our analyses we predict that a pathological situation in which I_{NaL} is further enhanced would increase the size of the safety zone. Indeed, if the enhanced I_{NaL} has a major role in generating the biomarker parameter, then a specific blocker of this current would tend to restore normal conditions.

Limitations of this study

We acknowledge several limitations of our approach at this stage of its development. Caution should be exercised when placing a data set in the safety plots if the simulations have been conducted at different stimulation frequencies. The efficacy of a drug can change significantly with heart rate.[67] In the case of ranolazine, the

observed I_{Kr} block is independent of stimulus frequency,[68] whereas its IC_{50} for I_{NaL} decreases with increased frequency.[69] This property was not evaluated in our approach because the required data for GS967 block at different frequencies are not available. After the IC_{50} changes as a function of stimulation frequency of a specific drug have been specified, this drug can be correctly positioned in the safety plot and the effects on the different biomarkers can be evaluated.

We also acknowledge that, as pointed out by consensus from the Cardiac Physiome Initiative,[70,71] development of complex models can include propagation of errors or uncertaincy in (i) data selection (ii) interpolation or (iii) interpretation. It was principally for these reasons that we selected the ORd model as the fundamental computation platform. The experimental data used to build the model are from the human heart and are very extense. Nonetheless, the ORd model was developed to model normal physiological AP waveforms, and considers the controversial presence of a large number of M cells in a ventricular strand.[72] Our application extends this data set to a substrate that is a target for clinical anti-arrhythmic agents or drug candidates new in development.

We conclude that safety plots can provide a very valuable tool in the initial phases of drug development, specifically in the preclinical assessment of the arrhythmogenic risk of compounds that block a number of different ion channels. This tool not only overcomes many limitations of experimentation, but also its predictive capacity allows a better selection of experiments, reducing the cost of drug screening.

METHODS

Human Ventricular Myocyte Model

Simulations of the electrical activity of an endocardial human ventricular myocyte were carried out using the human ventricular AP model developed by O'Hara et al.[31] (ORd). This model is based on experimental data taken from 140 healthy human hearts; it encompasses the formulation of 18 ionic currents and carrier-mediated fluxes and a detailed formulation of steady-state and transient ion concentrations, including intracellular Ca^{2+} transients. This model reproduces the electrophysiological behavior of all three types of human ventricular myocytes, with a high degree of fidelity, including alterations due to drug effects.

We have modified the formulation of I_{NaL} in ORd model to closely match experimental data from Maltsev et al.[73] In their experiments on human ventricular myocytes, I_{NaL}/I_{NaT} (I_{NaT} denotes peak I_{Na}) ratio was approximately 0.1% . In our model, the maximum conductance (g_{NaL}) was fitted accordingly using voltage clamp simulations, yielding 0.018 mS/μF. The new APD_{90} remains within experimental values.[72,74,75] Details are given in the supplemental material (Figure S1).

This I_{NaL} formulation was modified to simulate the effects of pathological conditions. Specifically, g_{NaL} was enhanced 2-fold, as a surrogate for a genetic modification of the human I_{Na}, which results in enhanced I_{NaL} and has been denoted LQT3 syndrome,[76] or to simulate part of the effects of free radical challenge,[48,50] heart failure,[77,78] or hypoxia.[49,51] We refer to this single modification of the ORd model as "baseline conditions" throughout the paper.

All model equations and code were taken from O'Hara et al.,[31] which can be downloaded from http://rudylab.wustl.edu. Rapid integration methods are provided in the Supplemental Materials from O'Hara et al.[31] For simulation of the basic human model, we used C++ code run on an array of Dell cluster nodes with 64-bit AMD Opteron processors, running Linux and Sun Microsystems Grid Engine.

Human Ventricular Strand Model

1-dimensional simulations of AP initiation and conduction were performed using a heterogeneous multicellular strand, which resembles some functional features of a

ventricular transmural wedge preparation, as described in O'Hara et al. [31] This strand was composed by 60 endocardial, 45 M, and 65 epicardial cells.

Drugs

The two drugs that have been evaluated in this study are ranolazine and GS967 (6-(4-(trifluoromethoxy) phenyl)-3-(trifluoromethyl)-[1,2,4]triazolo[4,3-a]pyridine), a potent and selective inhibitor of I_{NaL}.[10] Ranolazine has a potency of inhibition (IC_{50}) of 6 and 12 μM for the block of I_{NaL} and I_{Kr}, respectively,[56] and IC_{50} values for GS967 are 0.13 and >10 μM for the block of I_{NaL} and I_{Kr}, respectively. These values were obtained in rabbit ventricular myocytes, as detailed in Belardinelli et al.[10]

In this study a large number of inter-related sets of simulations were carried out. In each, the hypothetical potential drugs were "applied" in selected combinations arranged according to IC_{50} for I_{NaL} and I_{Kr}. The ranges of 10^{-7} to 10^{-3} M (pIC_{50} from 7 to 3) and 10^{-6} to 10^{-3} M (pIC_{50} from 6 to 3), were assessed respectively for I_{NaL} and I_{Kr}. The pharmaceutical description pIC_{50} (standing for -log IC_{50}) was used. To simulate the steady-state effects of these drugs, I_{NaL} and I_{Kr} conductances were reduced with a multiplicative factor (1-b), related to the IC_{50} as follows:

$$b = \frac{1}{1+\frac{IC_{50}}{[D]}} \qquad (1)$$

where [D] stands for the concentration of the potential drug. This value is 5 μM in our simulations, which is within the therapeutic concentration for ranolazine (1 to 10 μM).[79]

Parameter Definitions

All APs or other output parameters were measured after achieving steady-state conditions. Steady-state was then defined with an error of 1.9% in APD_{90} after 100

stimulation pulses. Each applied stimulus was 1.5 the threshold and 2 ms in duration. In the strand simulations, the stimuli were applied at the endocardial end of the fiber. Stimulation rate was varied in some of the single myocyte simulations, and was 1 Hz in 1D-fiber simulations.

Several accepted biomarkers for arrhythmic risk were calculated in our set of simulations: APD, triangulation, APD rate-dependence (RD), QT_{int}, and transmural dispersion of repolarization. APD values were determined at 90%, 60%, and 30% of repolarization and are referred as APD_{90}, APD_{60}, and APD_{30}, respectively. By convention[24] triangulation was defined as the difference between APD_{90} and APD_{30}. APD rate-dependence was calculated as the maximum APD_{90} (corresponding to the minimum frequency of stimulation of 0.5 Hz) minus the minimum APD_{90} (corresponding to the maximum frequency of stimulation of 2 Hz). In the multicellular simulations pseudo-ECGs were computed as described in O'Hara et al.[31] and the corresponding QT intervals were measured. Finally, repolarization time (RT) in the selected myocytes of the fiber was computed as the sum of the activation time and the APD_{90} of this cell. Based on this, transmural dispersion of repolarization was defined as the difference between the maximum and the minimum repolarization times along the heterogeneous fiber.

Ionic currents I_{NaL}, I_{Kr}, the slow component of the delayed rectifier potassium current (I_{Ks}), and the inward rectifier K^+ current (I_{K1}) were also measured. Importantly, net current (I_{net}) was determined as the sum of all ionic currents in the ORd model. This current was continuously measured during the AP (Figure 1 panel E). I_{net} was also calculated at a specific instant of time within the AP repolarization phase, i.e. 60% of repolarization (see Figure 3).

Safety Plot Construction

We have developed an approach to summarize and illustrate the results of the required complete set of simulations. The effects of potential drugs, having different specificities for I_{NaL} and I_{Kr}, on a specific biomarker (APD, triangulation, rate-dependence, QT_{int} or transmural dispersion of repolarization) can be illustrated on the plot. This has been achieved by constructing a color coded map denoted "safety plot" (see Figures 4, 5, 6, 8, and S2). Each safety plot illustrates the values of the chosen biomarker (e.g. APD_{90}) in a color coded scale as a function of the pIC_{50} values for I_{Kr} (horizontal axis) and I_{NaL} (vertical axis). The simulations were carried out for a fixed concentration of the potential drugs (5 μM). Thus, the block amount of both currents could be calculated from the correspondent pIC_{50}. The resulting sets of biomarker values relate molecular pharmacology actions at steady-state to accepted experimental and/or clinical measures of electrophysiological effect on APD_{90} or QT_{int}. This information is coupled with knowledge of regulatory agency standards for drug-induced changes (denoted by black lines). All simulations were performed under pathological conditions (with enhanced I_{NaL}).

ACKNOWLEDGEMENTS

This work was supported by: (i) Plan Nacional de Investigación Científica, Desarrollo e Innovación Tecnológica, (ii) Plan Avanza en el marco de la Acción Estratégica de Telecomunicaciones y Sociedad de la Información del Ministerio de Industria Turismo y Comercio of Spain (TSI-020100-2010-469), (iii) Programa de Apoyo a la Investigación y Desarrollo (PAID-06-11-2002) de la Universidad Politécnica de Valencia, (iv) Programa Prometeo (PROMETEO/2012/030) de la Consellería d'Educació Formació I Ocupació, Generalitat Valenciana, and (v) Gilead Sciences, Ltd.

REFERENCES

1. Maltsev VA, Silverman N, Sabbah HN, Undrovinas AI. Chronic heart failure slows late sodium current in human and canine ventricular myocytes: implications for repolarization variability. Eur J Heart Fail 2007;9(3):219-227.

2. Zaza A, Belardinelli L, Shryock JC. Pathophysiology and pharmacology of the cardiac "late sodium current.". Pharmacol Ther 2008;119(3):326-339.

3. Song Y, Shryock JC, Wagner S, Maier LS, Belardinelli L. Blocking late sodium current reduces hydrogen peroxide-induced arrhythmogenic activity and contractile dysfunction. J Pharmacol Exp Ther 2006;318(1):214-222.

4. Milberg P, Pott C, Fink M, Frommeyer G, Matsuda T, Baba A, et al. Inhibition of the Na+/Ca2+ exchanger suppresses torsades de pointes in an intact heart model of long QT syndrome-2 and long QT syndrome-3. Heart Rhythm 2008;5(10):1444-1452.

5. Jia S, Lian J, Guo D, Xue X, Patel C, Yang L, et al. Modulation of the late sodium current by ATX-II and ranolazine affects the reverse use-dependence and proarrhythmic liability of IKr blockade. Br J Pharmacol 2011;164(2):308-316.

6. Undrovinas AI, Belardinelli L, Undrovinas NA, Sabbah HN. Ranolazine improves abnormal repolarization and contraction in left ventricular myocytes of dogs with heart failure by inhibiting late sodium current. J Cardiovasc Electrophysiol 2006;17 Suppl 1):S169-S177.

7. Wu L, Shryock JC, Song Y, Li Y, Antzelevitch C, Belardinelli L. Antiarrhythmic effects of ranolazine in a guinea pig in vitro model of long-QT syndrome. J Pharmacol Exp Ther 2004;310(2):599-605.

8. Moss AJ, Zareba W, Schwarz KQ, Rosero S, McNitt S, Robinson JL. Ranolazine shortens repolarization in patients with sustained inward sodium current due to type-3 long-QT syndrome. J Cardiovasc Electrophysiol 2008;19(12):1289-1293.

9. Song Y, Shryock JC, Wu L, Belardinelli L. Antagonism by ranolazine of the pro-arrhythmic effects of increasing late INa in guinea pig ventricular myocytes. J Cardiovasc Pharmacol 2004;44(2):192-199.

10. Belardinelli L, Liu G, Smith-Maxwell C, Wang WQ, El-Bizri N, Hirakawa R, et al. A novel, potent, and selective inhibitor of cardiac late sodium current suppresses experimental arrhythmias. J Pharmacol Exp Ther 2013;344(1):23-32.

11. Banyasz T, Koncz R, Fulop L, Szentandrassy N, Magyar J, Nanasi PP. Profile of I(Ks) during the action potential questions the therapeutic value of I(Ks) blockade. Curr Med Chem 2004;11(1):45-60.

12. Carro J, Rodriguez JF, Laguna P, Pueyo E. A human ventricular cell model for investigation of cardiac arrhythmias under hyperkalaemic conditions. Philos Transact A Math Phys Eng Sci 2011;369(1954):4205-4232.

13. Fink M, Giles WR, Noble D. Contributions of inwardly rectifying K+ currents to repolarization assessed using mathematical models of human ventricular myocytes. Philos Transact A Math Phys Eng Sci 2006;364(1842):1207-1222.

14. Hopenfeld B. A mathematical analysis of the action potential plateau duration of a human ventricular myocyte. J Theor Biol 2006;240(2):311-322.

15. Maleckar MM, Greenstein JL, Giles WR, Trayanova NA. Electrotonic coupling between human atrial myocytes and fibroblasts alters myocyte excitability and repolarization. Biophys J 2009;97(8):2179-2190.

16. Nygren A, Fiset C, Firek L, Clark JW, Lindblad DS, Clark RB, et al. Mathematical model of an adult human atrial cell: the role of K+ currents in repolarization. Circ Res 1998;82(1):63-81.

17. Viswanathan PC, Rudy Y. Pause induced early afterdepolarizations in the long QT syndrome: a simulation study. Cardiovasc Res 1999;42(2):530-542.

18. Wu R, Patwardhan A. Effects of rapid and slow potassium repolarization currents and calcium dynamics on hysteresis in restitution of action potential duration. J Electrocardiol 2007;40(2):188-199.

19. Zaniboni M. 3D current-voltage-time surfaces unveil critical repolarization differences underlying similar cardiac action potentials: A model study. Math Biosci 2011;233(2):98-110.

20. Zaniboni M. Late phase of repolarization is autoregenerative and scales linearly with action potential duration in mammals ventricular myocytes: a model study. IEEE Trans Biomed Eng 2012;59(1):226-233.

21. Zaniboni M, Riva I, Cacciani F, Groppi M. How different two almost identical action potentials can be: a model study on cardiac repolarization. Math Biosci 2010;228(1):56-70.

22. Belardinelli L, Antzelevitch C, Vos MA. Assessing predictors of drug-induced torsade de pointes. Trends Pharmacol Sci 2003;24(12):619-625.

23. Shah RR, Hondeghem LM. Refining detection of drug-induced proarrhythmia: QT interval and TRIaD. Heart Rhythm 2005;2(7):758-772.

24. Hondeghem LM, Carlsson L, Duker G. Instability and triangulation of the action potential predict serious proarrhythmia, but action potential duration prolongation is antiarrhythmic. Circulation 2001;103(15):2004-2013.

25. Mirams GR, Cui Y, Sher A, Fink M, Cooper J, Heath BM, et al. Simulation of multiple ion channel block provides improved early prediction of compounds' clinical torsadogenic risk. Cardiovasc Res 2011;91(1):53-61.

26. Obiol-Pardo C, Gomis-Tena J, Sanz F, Saiz J, Pastor M. A multiscale simulation system for the prediction of drug-induced cardiotoxicity. J Chem Inf Model 2011;51(2):483-492.

27. Suzuki S, Murakami S, Tsujimae K, Findlay I, Kurachi Y. In silico risk assessment for drug-induction of cardiac arrhythmia. Prog Biophys Mol Biol 2008;98(1):52-60.

28. Mirams GR, Davies MR, Cui Y, Kohl P, Noble D. Application of cardiac electrophysiology simulations to pro-arrhythmic safety testing. Br J Pharmacol 2012;167(5):932-945.

29. Sarkar AX, Sobie EA. Quantification of repolarization reserve to understand interpatient variability in the response to proarrhythmic drugs: a computational analysis. Heart Rhythm 2011;8(11):1749-1755.

30. Weirich J, Antoni H. Rate-dependence of antiarrhythmic and proarrhythmic properties of class I and class III antiarrhythmic drugs. Basic Res Cardiol 1998;93 Suppl 1):125-132.

31. O'Hara T, Virag L, Varro A, Rudy Y. Simulation of the undiseased human cardiac ventricular action potential: model formulation and experimental validation. PLoS Comput Biol 2011;7(5):e1002061.

32. Wu L, Ma J, Li H, Wang C, Grandi E, Zhang P, et al. Late Sodium Current Contributes to the Reverse Rate-Dependent Effect of IKr Inhibition on Ventricular Repolarization. Circulation 2011;123(16):1713-1720.

33. Banyasz T, Barandi L, HArmati G, Virag L, Szentandrassy N, Marton I, et al. Mechanism of reverse rate-dependent action of cardioactive agents. Curr Med Chem 2011;18(24):3597-3606.

34. Noble D and Tsien RW (1972). The repolarization process of heart cells , in Electrical phenomena in the heart (ed. W. C. DeMello), pp. 133-161. New York: Academic Press.

35. Fink M, Noble D, Virag L, Varro A, Giles WR. Contributions of HERG K(+) current to repolarization of the human ventricular action potential. Prog Biophys Mol Biol 2008;96(1-3):357-376.

36. Goineau S, Castagne V, Guillaume P, Froget G. The comparative sensitivity of three in vitro safety pharmacology models for the detection of lidocaine-induced cardiac effects. J Pharmacol Toxicol Methods 2012;66(1):52-58.

615 37. Wu L, Guo D, Li H, Hackett J, Yan GX, Jiao Z, et al. Role of late sodium current
616 in modulating the proarrhythmic and antiarrhythmic effects of quinidine. Heart
617 Rhythm 2008;5(12):1726-1734.

618 38. Diness JG, Hansen RS, Nissen JD, Jespersen T, Grunnet M. Antiarrhythmic effect
619 of IKr activation in a cellular model of LQT3. Heart Rhythm 2009;6(1):100-106.

620 39. Laursen M, Olesen SP, Grunnet M, Mow T, Jespersen T. Characterization of
621 cardiac repolarization in the Gottingen minipig. J Pharmacol Toxicol Methods
622 2011;63(2):186-195.

623 40. Hondeghem LM. Thorough QT/QTc not so thorough: removes torsadogenic
624 predictors from the T-wave, incriminates safe drugs, and misses profibrillatory
625 drugs. J Cardiovasc Electrophysiol 2006;17(3):337-340.

626 41. Hondeghem LM, Snyders DJ. Class III antiarrhythmic agents have a lot of
627 potential but a long way to go. Reduced effectiveness and dangers of reverse use
628 dependence. Circulation 1990;81(2):686-690.

629 42. Bril A, Forest MC, Cheval B, Faivre JF. Combined potassium and calcium
630 channel antagonistic activities as a basis for neutral frequency dependent increase
631 in action potential duration: comparison between BRL-32872 and azimilide.
632 Cardiovasc Res 1998;37(1):130-140.

633 43. Jurkiewicz NK, Sanguinetti MC. Rate-dependent prolongation of cardiac action
634 potentials by a methanesulfonanilide class III antiarrhythmic agent. Specific block
635 of rapidly activating delayed rectifier K+ current by dofetilide. Circ Res
636 1993;72(1):75-83.

637 44. O'Hara T, Rudy Y. Quantitative comparison of cardiac ventricular myocyte
638 electrophysiology and response to drugs in human and nonhuman species. Am J
639 Physiol Heart Circ Physiol 2012;302(5):H1023-H1030.

640 45. Stengl M, Volders PG, Thomsen MB, Spatjens RL, Sipido KR, Vos MA.
641 Accumulation of slowly activating delayed rectifier potassium current (IKs) in
642 canine ventricular myocytes. J Physiol 2003;551(Pt 3):777-786.

643 46. Shah RR. The significance of QT interval in drug development. Br J Clin
644 Pharmacol 2002;54(2):188-202.

645 47. Nuyens D, Stengl M, Dugarmaa S, Rossenbacker T, Compernolle V, Rudy Y, et
646 al. Abrupt rate accelerations or premature beats cause life-threatening arrhythmias
647 in mice with long-QT3 syndrome. Nat Med 2001;7(9):1021-1027.

648 48. Gautier M, Zhang H, Fearon IM. Peroxynitrite formation mediates LPC-induced
649 augmentation of cardiac late sodium currents. J Mol Cell Cardiol 2008;44(2):241-
650 251.

651 49. Fearon IM, Brown ST. Acute and chronic hypoxic regulation of recombinant
652 hNa(v)1.5 alpha subunits. Biochem Biophys Res Commun 2004;324(4):1289-
653 1295.

654 50. Ward CA, Giles WR. Ionic mechanism of the effects of hydrogen peroxide in rat
655 ventricular myocytes. J Physiol 1997;500 (Pt 3)):631-642.

656 51. Saint DA. The cardiac persistent sodium current: an appealing therapeutic target?
657 Br J Pharmacol 2008;153(6):1133-1142.
658
659 52. Zygmunt AC, Eddlestone GT, Thomas GP, Nesterenko VV, Antzelevitch C.
660 Larger late sodium conductance in M cells contributes to electrical heterogeneity
661 in canine ventricle. Am J Physiol Heart Circ Physiol 2001;281(2):H689-H697.

662 53. Trenor B, Cardona K, Gomez JF, Rajamani S, Ferrero JM, Jr., Belardinelli L, et
663 al. Simulation and mechanistic investigation of the arrhythmogenic role of the late
664 sodium current in human heart failure. PLoS One 2012;7(3):e32659.

665 54. Wasserstrom JA, Salata JJ. Basis for tetrodotoxin and lidocaine effects on action
666 potentials in dog ventricular myocytes. Am J Physiol 1988;254(6 Pt 2):H1157-
667 H1166.

668 55. Martin RL, McDermott JS, Salmen HJ, Palmatier J, Cox BF, Gintant GA. The
669 utility of hERG and repolarization assays in evaluating delayed cardiac
670 repolarization: influence of multi-channel block. J Cardiovasc Pharmacol
671 2004;43(3):369-379.

672 56. Antzelevitch C, Belardinelli L, Zygmunt AC, Burashnikov A, Di Diego JM, Fish
673 JM, et al. Electrophysiological effects of ranolazine, a novel antianginal agent
674 with antiarrhythmic properties. Circulation 2004;110(8):904-910.

675 57. Noble D, Noble PJ. Late sodium current in the pathophysiology of cardiovascular
676 disease: consequences of sodium-calcium overload. Heart 2006;92 Suppl 4):iv1-
677 iv5.

678 58. Scirica BM, Morrow DA, Hod H, Murphy SA, Belardinelli L, Hedgepeth CM, et
679 al. Effect of ranolazine, an antianginal agent with novel electrophysiological
680 properties, on the incidence of arrhythmias in patients with non ST-segment
681 elevation acute coronary syndrome: results from the Metabolic Efficiency With
682 Ranolazine for Less Ischemia in Non ST-Elevation Acute Coronary Syndrome
683 Thrombolysis in Myocardial Infarction 36 (MERLIN-TIMI 36) randomized
684 controlled trial. Circulation 2007;116(15):1647-1652.

685 59. Hoefen R, Reumann M, Goldenberg I, Moss AJ, Uchi J, Gu Y, et al. In Silico
686 Cardiac Risk Assessment in Patients With Long QT Syndrome: Type 1: Clinical
687 Predictability of Cardiac Models. J Am Coll Cardiol 2012;60(21):2182-2191.

688 60. Silva JR, Pan H, Wu D, Nekouzadeh A, Decker KF, Cui J, et al. A multiscale
689 model linking ion-channel molecular dynamics and electrostatics to the cardiac
690 action potential. Proc Natl Acad Sci U S A 2009;106(27):11102-11106.

691 61. Starmer CF, Nesterenko VV, Undrovinas AI, Grant AO, Rosenshtraukh LV.
692 Lidocaine blockade of continuously and transiently accessible sites in cardiac
693 sodium channels. J Mol Cell Cardiol 1991;23 Suppl 1):73-83.

694 62. Rudy Y, Silva JR. Computational biology in the study of cardiac ion channels and
695 cell electrophysiology. Q Rev Biophys 2006;39(1):57-116.

696 63. Clancy CE, Zhu ZI, Rudy Y. Pharmacogenetics and anti-arrhythmic drug therapy:
697 a theoretical investigation. Am J Physiol Heart Circ Physiol 2007;292(1):H66-
698 H75.

699 64. Zygmunt AC, Nesterenko VV, Rajamani S, Hu D, Barajas-Martinez H,
700 Belardinelli L, et al. Mechanisms of atrial-selective block of Na channels by
701 ranolazine: I. Experimental analysis of the use-dependent block. Am J Physiol
702 Heart Circ Physiol 2011;301(4):H1606-H1614.

703 65. Nesterenko VV, Zygmunt AC, Rajamani S, Belardinelli L, Antzelevitch C.
704 Mechanisms of atrial-selective block of Na channels by ranolazine: II. Insights
705 from a mathematical model. Am J Physiol Heart Circ Physiol 2011;301(4):H1615-
706 H1624.

707 66. Zemzemi N, Bernabeu MO, Saiz J, Cooper J, Pathmanathan P, Mirams GR, et al.
708 Computational assessment of drug-induced effects on the electrocardiogram: from
709 ion channel to body surface potentials. Br J Pharmacol 2013;168(3):718-733.

710 67. Hille, B. (1992). Ionic channels in excitable membranes. Ed. Sinauer Associates,
711 Sunderland MA.

712 68. Rajamani S, Shryock JC, Belardinelli L. Rapid kinetic interactions of ranolazine
713 with HERG K+ current. J Cardiovasc Pharmacol 2008;51(6):581-589.

714 69. Rajamani S, El-Bizri N, Shryock JC, Makielski JC, Belardinelli L. Use-dependent
715 block of cardiac late Na(+) current by ranolazine. Heart Rhythm 2009;6(11):1625-
716 1631.

717 70. Bassingthwaighte J, Hunter P, Noble D. The Cardiac Physiome: perspectives for
718 the future. Exp Physiol 2009;94(5):597-605.

719 71. Quinn TA, Granite S, Allessie MA, Antzelevitch C, Bollensdorff C, Bub G, et al.
720 Minimum Information about a Cardiac Electrophysiology Experiment (MICEE):
721 standardised reporting for model reproducibility, interoperability, and data
722 sharing. Prog Biophys Mol Biol 2011;107(1):4-10.

72. Glukhov AV, Fedorov VV, Lou Q, Ravikumar VK, Kalish PW, Schuessler RB, et al. Transmural dispersion of repolarization in failing and nonfailing human ventricle. Circ Res 2010;106(5):981-991.

73. Maltsev VA, Undrovinas AI. A multi-modal composition of the late Na+ current in human ventricular cardiomyocytes. Cardiovasc Res 2006;69(1):116-127.

74. Li GR, Feng J, Yue L, Carrier M. Transmural heterogeneity of action potentials and Ito1 in myocytes isolated from the human right ventricle. Am J Physiol 1998;275(2 Pt 2):H369-H377.

75. Drouin E, Charpentier F, Gauthier C, Laurent K, Le Marec H. Electrophysiologic characteristics of cells spanning the left ventricular wall of human heart: evidence for presence of M cells. J Am Coll Cardiol 1995;26(1):185-192.

76. Berecki G, Zegers JG, Bhuiyan ZA, Verkerk AO, Wilders R, van Ginneken AC. Long-QT syndrome-related sodium channel mutations probed by the dynamic action potential clamp technique. J Physiol 2006;570(Pt 2):237-250.

77. Maltsev VA, Silverman N, Sabbah HN, Undrovinas AI. Chronic heart failure slows late sodium current in human and canine ventricular myocytes: implications for repolarization variability. Eur J Heart Fail 2007;9(3):219-227.

78. Valdivia CR, Chu WW, Pu J, Foell JD, Haworth RA, Wolff MR, et al. Increased late sodium current in myocytes from a canine heart failure model and from failing human heart. J Mol Cell Cardiol 2005;38(3):475-483.

79. Belardinelli L, Shryock JC, Fraser H. Inhibition of the late sodium current as a potential cardioprotective principle: effects of the late sodium current inhibitor ranolazine. Heart 2006;92 Suppl 4):iv6-iv14.

80. Chang CC, Acharfi S, Wu MH, Chiang FT, Wang JK, Sung TC, et al. A novel SCN5A mutation manifests as a malignant form of long QT syndrome with perinatal onset of tachycardia/bradycardia. Cardiovasc Res 2004;64(2):268-278.

FIGURE LEGENDS

Figure 1. Illustrations of the three main sets of conditions that are analyzed in these simulations of the ventricular action potential (AP). The top row (A) shows APs computed at 1 Hz in response to baseline conditions (left); baseline plus ranolazine (centre), and a novel ranolazine derivative, GS967 (right). Note that in all calculations the baseline condition is intended to mimic the enhanced I_{NaL}, which is a hallmark feature of LQT3 syndrome.[80] Thus, I_{NaL} was increased 2-fold over the value in the control conditions. The dashed line shows control AP. Panel B shows baseline I_{NaL} (left) and reductions in the current following steady-state effects of ranolazine or GS967. Panel C shows the relative sizes and approximate time course of the two time and voltage-dependent K^+ currents in human ventricle. Note the difference in current scales for I_{Kr} versus I_{Ks}. Panel D illustrates the inwardly rectifying backgroud K^+ current I_{K1}. In panel E the net outward current during the plateau and repolarization phases of the AP are shown. The negative peak was truncated to better observe the shape of this current in a bigger scale. The dotted vertical lines provide reference points dennoting 30%, 60% and 90% of complete AP repolarization.

Figure 2. Effect of change in steady-state heart rate on drug-induced block of I_{NaL} and I_{Kr}. Action potentials (APs) (panel A), I_{NaL} (panel B), I_{Kr} (panel C), and I_{Ks} (panel D) at BCLs of 2000 and 500 ms (dashed and continuous traces, respectively) under selected conditions: (i) column 1 baseline conditions, (ii) drug 1 (more specific for I_{Kr}) in column 2, (iii) drug 2 (more specific for I_{NaL}) in column 3, and (iv) drug 3 (same specificity for I_{NaL} and I_{Kr}) in column 4.

776 **Figure 3.** Instantaneous net current measured at APD_{60} as a function of APD_{90} for
777 different combinations of I_{Kr}/I_{NaL} IC_{50} ratios (different symbols). For each curve,
778 corresponding to a specific combination of I_{Kr}/I_{NaL} IC_{50} ratio, simulations were
779 performed at increasing BCLs from 500 ms to 2000 ms in each curve. Baseline
780 corresponds to conditions where only I_{NaL} is enhanced two-fold and no drug is applied.
781
782 **Figure 4.** Illustration of combined effects of drugs (at 5 μM) which inhibit I_{Kr}, I_{NaL} or
783 both on APD_{90}. This "Safety Plot" is constructed using selected values of IC_{50} for I_{NaL}
784 blockers on the y-axis, and IC_{50}values of I_{Kr} block on the x-axis. The reference action
785 potentials (APs) shown are (1) baseline waveform at 1 Hz, (2) AP waveform after
786 complete block of only I_{NaL}, (3) AP waveform after complete block of only I_{Kr}, (4) AP
787 waveform resulting from an equal degree of block of I_{Kr} and I_{NaL}, and (5) AP waveform
788 after complete block of I_{NaL} and I_{Kr}. Black lines join IC_{50} combinations for which APD
789 is either increased or decreased by 10% or 20% with respect to the baseline APD shown
790 at the right bottom edge of this matrix. Baseline corresponds to conditions where only
791 I_{NaL} is enhanced two-fold.
792
793 **Figure 5.** 2D APD_{90} (panel A), APD_{60} (panel B), APD_{30} (panel C), and triangulation
794 (panel D) safety plots as a function of pIC_{50} for I_{Kr} (horizontal axis) and I_{NaL} (vertical
795 axis), for a drug concentration of 5 μM. Here the effects at steady-state of two
796 stimulation frequencies (BCL of 500 ms in the left and BCL of 1000 ms in the right) are
797 illustrated. Ranolazine is represented by the circle and GS967 by the triangle. Black
798 lines join IC_{50} combinations for which APD or triangulation is either increased or
799 decreased by 10% or 20% with respect to baseline APD or triangulation. As in Figure 4,

the baseline data are shown in the right bottom edge of the matrix, that is under conditions where only I_{NaL} is enhanced two-fold.

Figure 6. 2D maps of the effects of steady-state changes in cycle length. APD rate-dependence (RD) was measured as $APD_{(0.5\ Hz)}$-$APD_{(2\ Hz)}$. APD_{90} (panel A), APD_{60} (panel B), and APD_{30} (panel C) maps are shown. Black lines join IC_{50} combinations for which the effects of changes in the cycle length is increased or decreased by 10% or 20% with respect to the baseline data (again represented in the right bottom edge of the matrix, where only I_{NaL} is two-fold enhanced).

Figure 7. Panel A: action potentials (APs) in endocardial (continuous line), Midmyocardial (dashed line) and epicardial (dotted-dashed line) cells at baseline and after ranolazine (5 μM) and GS967 (5 μM). Panel B: pseudo-ECGs computed and measured as described in Methods. Panel C: Repolarization time (RT) profile along the transmural fiber under baseline conditions, and during steady-state effects of ranolazine (5 μM) and GS967 (5 μM). Repolarization times are shown at 90% of repolarization in these three tyopes of ventricular myocytes at baseline, and in the presence of 5 μM of Ranolazine and GS967. Transmural dispersion of repolarization (TDR) in ms is indicated for each case. Simulations were conducted at a BCL of 1000 ms.

Figure 8. Safety Plot analysis based on computed QT interval (QT_{int}) (panel A) or transmural dispersion of repolarization (TDR) (panel B), as a function of pIC_{50} for I_{Kr} (horizontal axis) and I_{NaL} (vertical axis). Drug concentrations of 3, 5 and 8 μM are considered. Ranolazine is represented by the circle and GS967 by the triangle. Black lines join IC_{50} combinations for which Qt_{int} or TDR increase or decrease by 10% or

825 20% with respect to baseline values, represented in the right bottom edge of the matrix,
826 i.e. where only I_{NaL} is enhanced two-fold. Simulations were conducted at a BCL of 1000
827 ms.
828
829
830
831
832

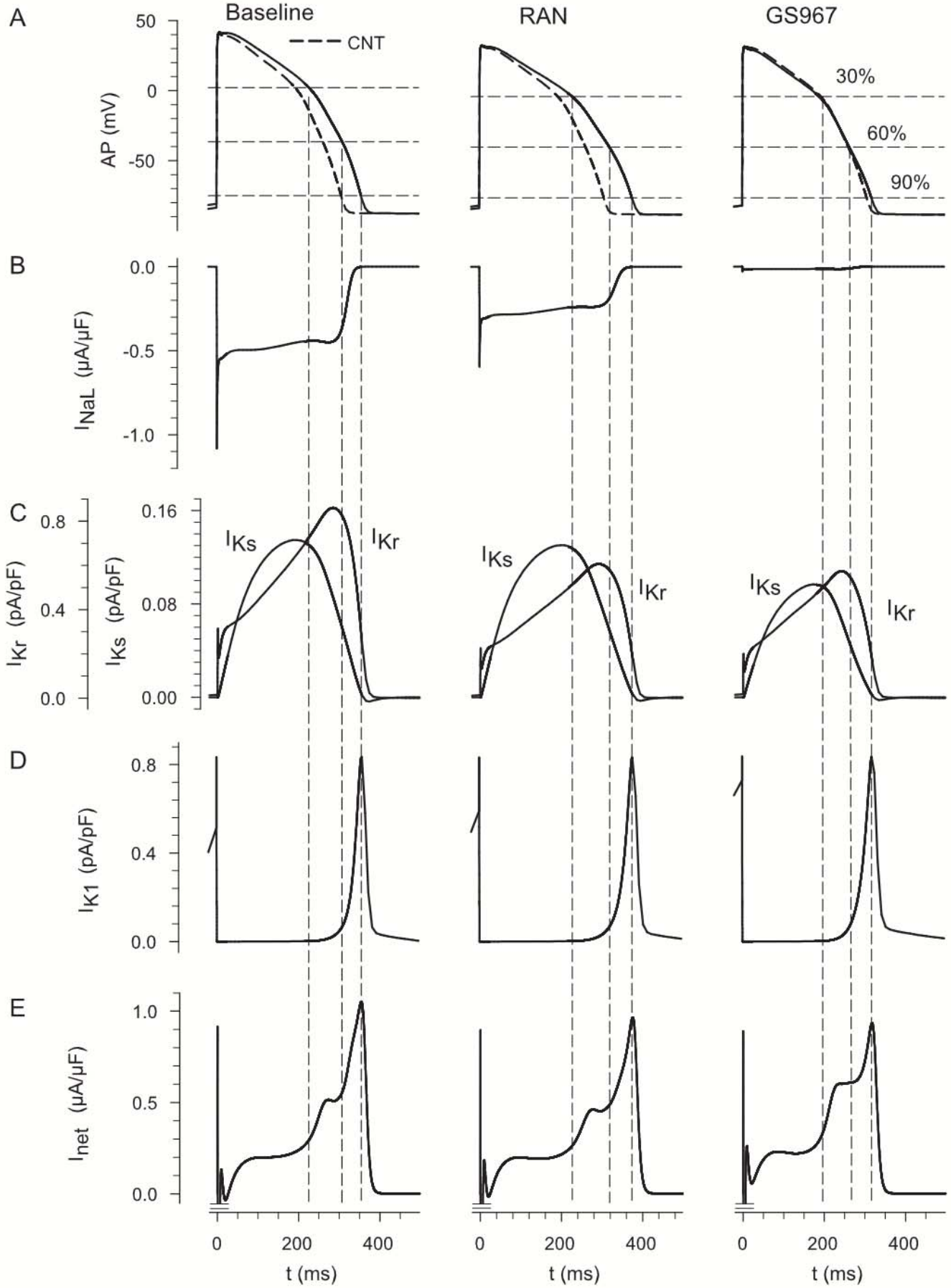
A
Baseline
RAN
GS967
CNT
AP (mV)
50
0
-50
30%
60%
90%
B
I_{NaL} (μA/μF)
0.0
-0.5
-1.0
C
I_{Kr} (pA/pF)
I_{Ks} (pA/pF)
0.8
0.4
0.0
0.16
0.08
0.00
I_{Ks}
I_{Kr}
D
I_{K1} (pA/pF)
0.8
0.4
0.0
E
I_{net} (μA/μF)
1.0
0.5
0.0
0
200
400
t (ms)

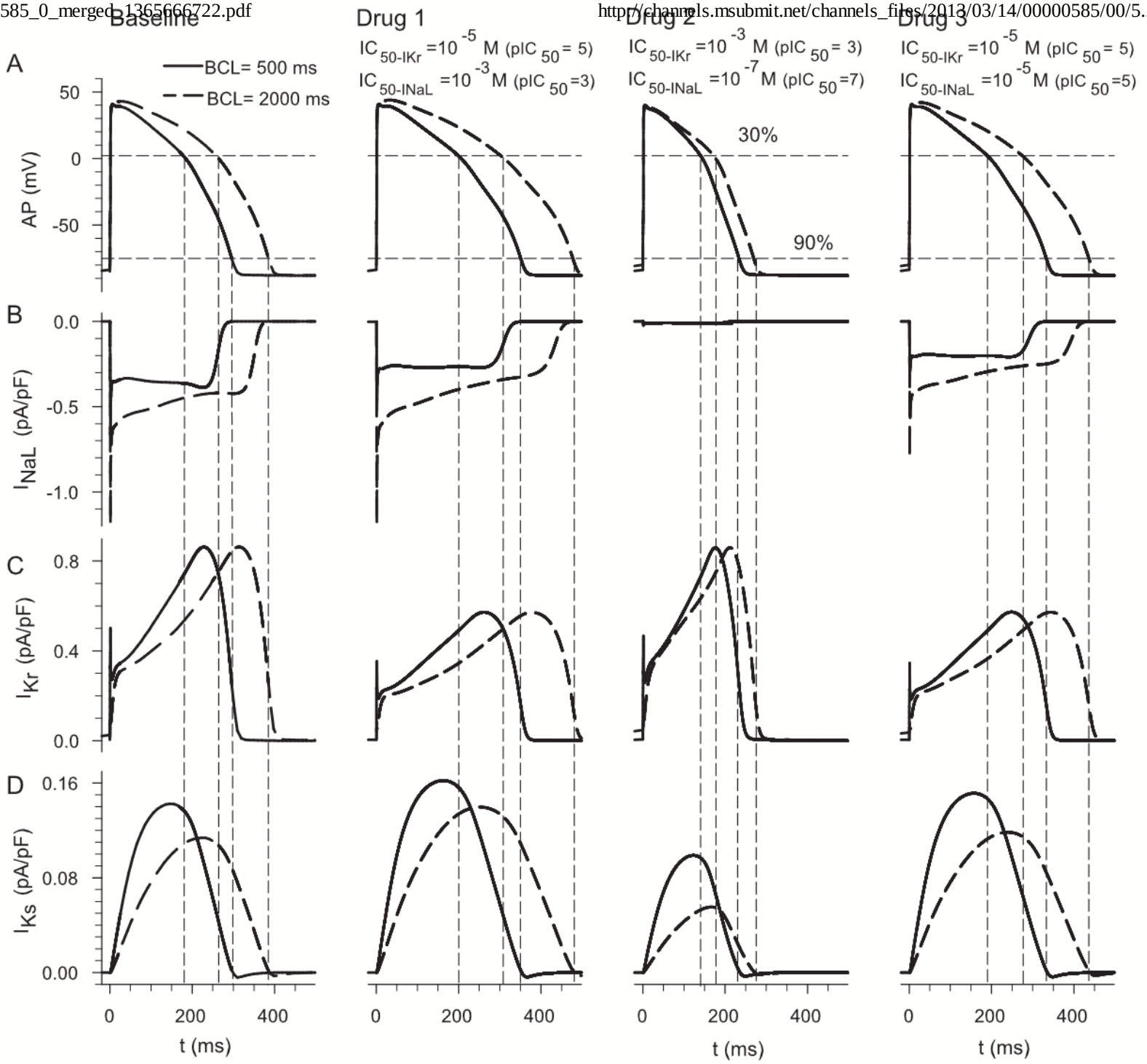
Baseline
Drug 1
Drug 2
Drug 3
A
BCL= 500 ms
BCL= 2000 ms
IC50-IKr =10-5 M (pIC50= 5)
IC50-INaL =10-3M (pIC50=3)
IC50-IKr =10-3 M (pIC50= 3)
IC50-INaL =10-7 M (pIC50=7)
IC50-IKr =10-5 M (pIC50= 5)
IC50-INaL =10-5M (pIC50=5)
30%
90%
AP (mV)
B
INaL (pA/pF)
C
IKr (pA/pF)
D
IKs (pA/pF)
t (ms)

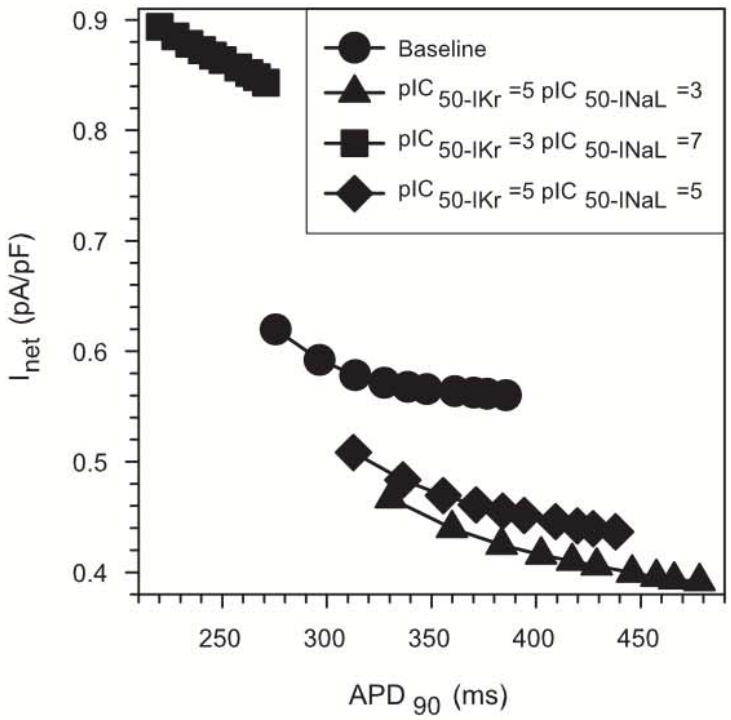
Baseline
pIC 50-IKr =5 pIC 50-INaL =3
pIC 50-IKr =3 pIC 50-INaL =7
pIC 50-IKr =5 pIC 50-INaL =5
0.9
0.8
0.7
0.6
0.5
0.4
I net (pA/pF)
250
300
350
400
450
APD 90 (ms)

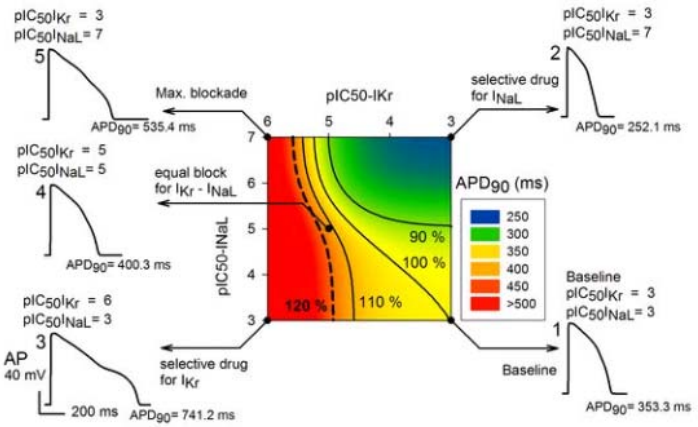
pIC50IKr = 3
pIC50INaL = 7
5
APD90 = 535.4 ms
Max. blockade
pIC50-IKr
selective drug for INaL
pIC50IKr = 3
pIC50INaL = 7
2
APD90 = 252.1 ms
pIC50IKr = 5
pIC50INaL = 5
4
APD90 = 400.3 ms
equal block for IKr - INaL
pIC50-INaL
APD90 (ms)
250
300
350
400
450
>500
90 %
100 %
110 %
120 %
pIC50IKr = 6
pIC50INaL = 3
3
AP
40 mV
200 ms
APD90 = 741.2 ms
selective drug for IKr
Baseline
Baseline
pIC50IKr = 3
pIC50INaL = 3
1
APD90 = 353.3 ms